Biomaterials Science

PAPER

View Article Online
View Journal | View Issue

Cite this: *Biomater. Sci.*, 2019, **7**, 1188

Second harmonic generation microscopy of collagen organization in tunable, environmentally responsive alginate hydrogels†

Anuraag Boddupalli[a] and Kaitlin M. Bratlie *[a,b,c]

We fabricated photocrosslinked, environmentally responsive alginate hydrogels for tissue engineering applications. Methacrylated alginate (ALGMA) hydrogels were prepared across a variety and combination of ionic and covalent (chain growth, step growth, and mixed mode) crosslinking strategies to obtain a range of compressive moduli from 9.3 ± 0.2 kPa for the softest ionically crosslinked hydrogels to 22.6 ± 0.3 kPa for the dually crosslinked ionic mixed mode gels. The swelling behavior of the alginate hydrogels was significantly higher under basic pH conditions. Stiffer gels consistently swelled to a lesser degree compared to softer gels for all conditions. These hydrogels were stable – retaining >80% of their original mass for three weeks – when incubated in a basic solution of diluted sodium hydroxide, which mimicked accelerated degradation conditions. Encapsulated NIH/3T3 fibroblasts remained viable and proliferated significantly more in stiffer hydrogel substrates compared to softer gels. Additionally, the collagen secreted by encapsulated fibroblasts was quantifiably compared using second harmonic generation (SHG) imaging. Fibroblasts encapsulated in the softer hydrogels secreted significantly less collagen than the stiffer gels. The collagen in these softer gels was also more aligned than the stiffer gels. The ability to tune collagen organization using hydrogels has potential applications ranging from corneal wound healing where organized collagen is desired to epithelial wound scaffolds where a random organization is preferable.

Received 27th November 2018,
Accepted 11th January 2019

DOI: 10.1039/c8bm01535j

rsc.li/biomaterials-science

1. Introduction

The human body contains natural tissue environments with dynamic and diverse mechanical properties.[1] Dynamic changes occur from regular maintenance of homeostasis, wound healing, or a response to implants.[2] Cells reside within these tissues ensconced in a three-dimensional scaffold known as the extracellular matrix (ECM), which responds to both macroscopic as well as microscopic perturbations.[3] The ECM is composed of different combinations of proteins like collagen, glycosaminoglycans, and adhesive glycoproteins which vary from organ to organ.[4] The macroscopic aspects derive from how the ECM provides structural integrity to the native tissue as well as a separation between different layers of tissue organization.[5] On a smaller scale, there are biochemical cues provided by the proteins that comprise the ECM, such as collagen and fibronectin, that can instigate diverse cell signaling pathways,[6,7] alter cell shape,[8] as well as changes in cytoskeletal organization,[1,9] and stress fiber formation.[10] These aspects of the cell-matrix interactions are influential for several critical processes including angiogenesis,[11] organogenesis,[12] wound healing,[13] as well as response to diseases[14] and tumor metastasis.[15]

The goal of tissue engineering is to recapitulate the natural, dynamic *in vivo* environment in order to minimize unwanted host responses as well as replicate lost tissue.[16] Tissue engineering covers not just the obvious motive of improving current healthcare solutions, but also to decrease costs associated with global healthcare, which is expected to rise to 8% of the US GDP by 2040.[17] An ideal material for tissue engineering scaffolds would be biocompatible, mechanically tunable, and have degradation rates that match those of tissue regeneration.[18,19] Natural polymers, with their similarity to the ECM are easy to obtain, modify, and apply to diverse tissue engineering applications.[20]

Alginate is an anionic polysaccharide which derives from seaweed or bacteria and has been effectively used as a support-

[a]*Department of Chemical & Biological Engineering, Iowa State University, Ames, Iowa 50011, USA. E-mail: kbratlie@iastate.edu; Fax: +1-515-294-5444; Tel: +1-515-294-7304*
[b]*Department of Materials Science & Engineering, Iowa State University, Ames, Iowa 50011, USA*
[c]*Division of Materials Sciences and Engineering, Ames National Laboratory, Ames, Iowa 50011, USA*

†Electronic supplementary information (ESI) available. See DOI: 10.1039/c8bm01535j

ing scaffold or tunable delivery system for tissue repair.[21] It can be easily crosslinked using divalent cations, as well as interact with a wide variety of proteoglycans and polyelectrolytes. The carboxylic acid moiety on alginate renders it pH-responsive and it can be used to deliver diverse payloads.[22] Unlike conventional cationic crosslinking of hydrogels, we explored covalent crosslinking facilitated by methacrylation of the alginate backbone so that alginate could be chemically crosslinked through photoinitiated mechanisms.[23] Covalently crosslinked hydrogels are more stable *in vivo*, unlike ionically crosslinked alginate which degrades rapidly due to preferential replacement of divalent cations by monovalent ones.[24] UV-crosslinkable methacrylated alginate (ALGMA) hydrogel formulations show structural stability, tunability of crosslinking mechanisms as well as significant cytocompatibility for use as cell-encapsulation platforms to study secretion of ECM proteins *in vitro*.[25,26] ECM proteins like collagen play a critical role in the structural integrity and cell–material interactions across a range of biological processes such as the fibrotic response to foreign bodies and wound healing.[27,28] Both fibroblasts and myofibroblasts secrete collagen types I and III, as a critical part of their mechanotransduction processes.[29] There is a need to understand the mechanisms through which stromal cells sense diverse materials and the kinetics of ECM protein secretion, particularly as to how dysregulation in collagen deposition has been linked to hypertrophic scars and keloid formation.[30,31] These studies inspired preparation of tunable alginate hydrogel environments that can be used for studying collagen organization under very soft, responsive conditions.[32]

Diverse crosslinking strategies can be employed to fabricate a range of materials properties of ALGMA hydrogels. Chain growth polymerization can be initiated using photoinitiators *via* Irgacure 2959 in a degassed solution of the hydrogel to form dense chains of methacrylated alginate networks.[33,34] Step growth polymerization occurs through thiol–ene photo-click chemistry wherein the free radical from the photo-initiator cleavage abstracts a proton from the thiol crosslinker to create a thiyl radical. Subsequent propagation of the step growth mechanism takes place through the reaction of the thiyl radical and the vinyl group.[35] A combination of step and chain growth mechanisms, termed mixed mode has been previously studied to prepare hybrid covalent crosslinks in the ALGMA solutions.[32,36,37] To further increase the range of mechanical properties, ionic crosslinking of the covalently crosslinked hydrogels has been done using naturally derived polymers like alginate,[38] carrageenan,[39] and hyaluronan.[40] Collagen secretion levels from encapsulated fibroblasts has been largely evaluated using fluorescent tagging or SDS-PAGE.[41,42] Second harmonic generation (SHG) microscopy allows for sensitive, high-content-imaging of not just secreted collagen, but also collagen organization.[43,44]

In this study, we use SHG microscopy and subsequent data analysis to examine how hydrogel stiffness can tune collagen organization from aligned to stochastic when encapsulating NIH/3T3 fibroblasts. The ability to influence collagen organization is a relatively unexplored area with previous research focused on visualizing the collagen alignment in neocartilage secreted by primary mesenchymal stem cells showing no direct cause-effect relationships.[45] We sought to decouple the effects of crosslinking density and compressive modulus, as well as crosslinking mechanism on how scaffolds influence remodeling by encapsulated fibroblasts. For specific applications such as skin grafts, cartilage repair, and corneal wound healing, being able to tune collagen organization to avoid compliance mismatch from the local microenvironment will further improve scaffolds by better recapitulating the native environment.

2. Experimental

2.1. Materials

Medium viscosity alginic acid (CAS 9005-38-3) was obtained from MP Biomedicals Fisher Scientific (Hampton, NH, USA) and methacrylic anhydride (CAS 760-93-00) was supplied by Sigma Aldrich (St Louis, MO, USA). 2-Hydroxy-4′-(2-hydroxyethoxy)-2-methylpropiophenone (Irgacure 2959) was obtained from Sigma-Aldrich and dithiothreitol (DTT) was obtained from VWR Chemicals (Batavia, IL, USA). Other materials were purchased through Sigma Aldrich and were used as received, unless otherwise stated. Fresh deionized water (Milli-Q, Thermo Scientific Nanopure, Waltham, MA, USA) was used throughout this study.

2.2. Methacrylated alginate (ALGMA) synthesis

Methacrylated alginate solutions were prepared based on a previously described protocol.[32] A 1% (w/v) solution of medium viscosity alginic acid in DI water was prepared by mixing 2 g alginic acid powder in 200 mL of DI water. Methacrylic anhydride (16 mL) was slowly added to the solution. The pH of the solution was maintained between 8 and 9 using aliquots of 5 M NaOH at 4 °C. After 24 h, the methacrylated alginate solution was dialyzed against water using a molecular weight cutoff membrane of 13 000 Da for two days with dialysate being refreshed twice daily. The final dialyzed product was lyophilized (4.5 L, Labconco, Kansas City, MO, USA). NMR was used to confirm methacrylation of the alginic acid. Solutions of alginate and ALGMA were prepared using standard protocols.[46] The % methacrylation was calculated by the relative integration of the protons from the methacrylate group (I_{CH_2} at δ = 6.0 and 5.6 ppm) and the methyl group (I_{CH_3} at δ = 1.8 ppm) to the protons from the carbohydrate peak ($I_{polymer}$) using eqn (1) (Fig. S1†).

$$\%\text{Methacrylation} = \frac{\left(\frac{I_{CH_2}}{n_{CH_2}} + \frac{I_{CH_3}}{n_{CH_3}}\right)}{\frac{I_{polymer}}{n_{H_{polymer}}}} \quad (1)$$

2.3. Hydrogel fabrication and characterization

The stock solution for methacrylated alginate hydrogels was prepared by dissolving 300 mg of ALGMA and 10 mg of

Irgacure 2959 in 10 mL of DI water. Step growth, chain growth and mixed mode polymerization was conducted to obtain a range of mechanically different hydrogels. The step growth polymerization was obtained by adding 250 μL of 4 mg mL^{-1} dithiothreitol (DTT) to the stock solution. Chain growth polymerization was conducted by degassing the stock solution under vacuum. Mixed mode polymerization was obtained by adding 250 μL of 4 mg mL^{-1} DTT followed by degassing. All hydrogels were crosslinked by exposure to UV light (365 nm, 2 W cm^{-2}) for 10 minutes. Dually crosslinked ALGMA hydrogels were fabricated by adding 100 μL of 0.2 M $SrCl_2$ after exposure to UV light.

To measure the compressive modulus of the ALGMA hydrogels, plugs (6 mm thick, 16 mm diameter, $n = 4$) were prepared for testing. These hydrogel samples were placed between two glass slides, on which sequential series of weights were added. Image J (NIH, Bethesda, MD, USA) was used to evaluate changes in height and cross-sectional area of the hydrogel samples in response to the weights. The slope of the linear region in the stress strain curve over a strain range of 5–15% was defined as the compressive modulus.

Swelling ratios of the different crosslinked hydrogels ($n = 3$) were measured after drying at room temperature. These hydrogels were swollen in acetate buffers (1 mM) and maintained at pH 3, 5, 7.4, and 9 for two days. The swelling ratios were subsequently calculated after analyzing the recorded dry and wet weights using eqn (2) where M_d is the dry mass and M_w is the wet mass.

$$\text{Swelling ratio} = \frac{M_w - M_d}{M_d} \quad (2)$$

2.4. *In vitro* degradation

To test the degradation of the hydrogels, the gels were placed under accelerated degradation conditions (0.1 mM NaOH). After equilibrating these gels for one day in solution, masses were recorded for each consecutive day. The % mass remaining was compared with the initial mass and recorded for each time-point.

2.5. Cell culture and proliferation assay

NIH/3T3 fibroblasts (ATCC, Manassas, VA, USA) were passaged at 37 °C with 5% CO_2 in Dulbecco's modified Eagle's medium (Cellgro, Thermo Scientific, Waltham, MA, USA) supplemented with 10% bovine calf serum, penicillin (100 U L^{-1}), and streptomycin (100 μg mL^{-1}), referred to as complete medium (CM). Cell suspension aliquots of 200 μL (1×10^7 cells per mL) were mixed 300 μL of the different hydrogel solutions and were pipetted into 48 well plates. For each plate, live and dead controls were made by plating cells directly on tissue culture plastic. The plates were incubated for 48 h. The medium in the dead control wells was aspirated and replaced with 300 μL of 70% ethanol for 10 minutes. Subsequently, the supernatant in all wells was aspirated. To each well 150 μL of working solution (2 μM calcein AM (AnaSpec, Fremont, CA, USA) and 7.5 μM of 7-aminoacinomycin D (Tonbo Biosciences, San Diego, CA, USA) in phosphate buffered saline (PBS)) was added and the plates were incubated for 30–40 min at 37 °C in 5% CO_2. Fluorescent images were taken using EVOS Floid Cell Image Station (Thermo Scientific) with the red (excitation/emission 586/646 nm) and green channels (482/532 nm) set to visualize the dead and live cells respectively. Live and dead cells were quantified at an excitation/emission of 485/528 nm and 645/490 nm, respectively, using a plate reader (BioTek Synergy HT Multidetection Microplate Reader, Biotek, Winooski, VT, USA). The percentage of live cells was determined using the following equation:

$$\%\text{live cells} = \frac{F(528)_{\text{sample}} - F(528)_{\text{dead control}}}{F(528)_{\text{live control}} - F(528)_{\text{dead control}}} \times 100\% \quad (3)$$

where $F(528)_{\text{sample}}$ is the fluorescent signal at 528 nm from the cell laden samples, $F(528)_{\text{dead control}}$ is the fluorescent signal at 528 nm from the lysed control samples, and $F(528)_{\text{live control}}$ is the fluorescent signal at 528 nm from the control samples.

2.6. Second harmonic generation microscopy of the gels

Equal volumes of suspended NIH/3T3 fibroblasts (1×10^7 cells per mL) were mixed with hydrogel solutions. The cell-gel suspension (100 μL) was pipetted between two coverslips, which were exposed to UV light (365 nm, 2 W cm^{-2}) for 10 min. These gelled samples were then placed in Petri dishes containing CM. Medium was replaced every three days. Negative controls were prepared by crosslinking the gels without cells. All samples were preserved in 10% formalin before imaging.

A mode-locked Ti:sapphire laser (100 fs pulse width, 1 kHz repetition rate obtained from Libra, Coherent, Santa Clara, CA, USA) that operates with an 800 nm fundamental, was used to image all samples. A half-wave plate and Glan-Thompson polarizer (Thorlabs, Newton, NJ, USA) was used to control the power at the sample stage. The second harmonic signal from the interaction with the samples was collected in transmission mode.

To image these samples, an inverted microscope (Amscope, Irvine, CA, USA) and a Nikon Plan Fluorite objective (20×, 0.50 NA, 2.1 mm WD, Nikon, Melville, NY, USA) was used to focus the beam. The SHG transmission was collected using a Nikon water immersion objective (40×, 0.8 NA, 3.5 mm WD, Nikon). This signal was reflected by a dichroic mirror (DMLP425 T, Thorlabs). Two short pass filters <450 nm (FGB37 M, Thorlabs) and an 808 nm notch filter (NF-808.0-E-25.0 M, Melles Griot, Rochester, NY, USA) were used to separate the signal from the fundamental beam prior to detection by the intensified charge couple device (iCCD, iStar 334T, Andor, Belfast, UK). A Glan-Thompson polarizer and a half-wave plate mounted on a motor-driven rotational stage (Thorlabs) was used to generate linear polarized light to conduct polarized SHG imaging. Images of the samples were acquired at every 10° from 0° to 350°. For every experimental condition, images were collected in triplicate. The regions of interest (ROIs) were analyzed and fit using the following equation:

$$I_{SHG} = c \cdot \left\{ \left[\sin^2(\theta_e - \theta_o) + \left(\frac{\chi_{zzz}}{\chi_{zxx}}\right) \cos^2(\theta_e - \theta_o) \right]^2 + \left(\frac{\chi_{xzx}}{\chi_{zxx}}\right)^2 \sin^2(2(\theta_e - \theta_o)) \right\} \quad (4)$$

where $\frac{\chi_{zzz}}{\chi_{zxx}}$ and $\frac{\chi_{xzx}}{\chi_{zxx}}$ are the second-order susceptibility tensor element ratios, θ_e and θ_o are the incident polarization angle and collagen fiber angle, respectively, and c is a normalization constant. Each ROI was individually analyzed for the orientation of collagen within it. A histogram was generated detailing the orientation of the collagen in the entire image. The organization of collagen was evaluated based on the full-width at half maximum (FWHM) of the Gaussian fit of the histogram.

2.7. Statistical analysis

Data generated was statistically analyzed and the values are reported as mean ± standard deviation (SD). Mean comparisons were determined to be statistically significant *via* a two-way ANOVA. Tukey's honest significant difference test was used to evaluate the pair-wise comparisons. Statistically significant differences were identified for $p < 0.05$.

3. Results

3.1. Characterization of ALGMA hydrogels

Characterization of the ALGMA was conducted using ^{1}H NMR spectroscopy (Fig. S1†), based on a previously described protocol.[47] Peaks appearing at 6.0 and 5.6 ppm were assigned to the methacrylamide protons confirming methacrylation of the alginic acid. The extent of methacrylation was calculated to be 27 ± 2% using eqn (1). The mannuronic acid content was determined to be 50 ± 2%.

3.2. Compressive moduli

The compressive modulus of medium viscosity ALGMA hydrogels was modulated *via* different crosslinking methods.[32] Comparisons of the compressive moduli of the different hydrogel preparations are shown in Fig. 1. Stiffness significantly increased from 9.3 ± 0.2 kPa for step growth, 13.0 ± 0.3 kPa for chain growth, and 15.2 ± 0.2 kPa for the mixed mode conditions. Dually crosslinked hydrogels were formed by incubating the hydrogels in 0.2 M $SrCl_2$ and had compressive moduli ~7 kPa higher than the covalently crosslinked gels. These gels had compressive moduli of 16.7 ± 0.3 kPa for ionic step growth, 20.2 ± 0.4 kPa for ionic chain growth, and 22.6 ± 0.3 kPa for the relatively stiffest formulation of the ionic mixed mode condition. The non-methacrylated ionic alginate hydrogels had a compression modulus of 8.3 ± 0.3 kPa. In comparison to the very low viscosity ALGMA hydrogels which showed a range of 0.7 ± 0.1 to 2.24 ± 0.1 kPa from our previous study,[32] these medium viscosity-based gels were significantly stiffer, thus depicting two completely different ranges of mechanical environment. These distinct ranges of mechanotransducive cues provide us with a good comparison of cell responses to stiff substrates (similar to what is observed for musculoskeletal environments[48,49]) and soft substrate (similar to fatty tissue in the liver[50] or healthy lung tissues[49,51]).

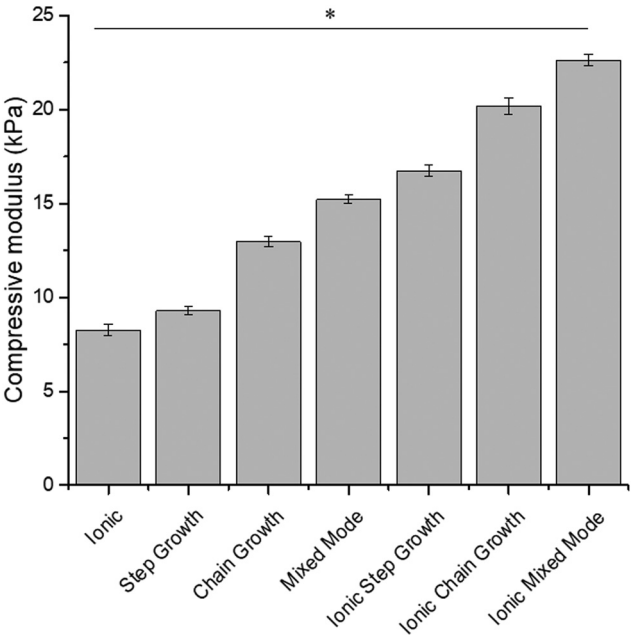

Fig. 1 Compressive moduli of medium viscosity alginate hydrogels. Compressive moduli of methacrylated alginate hydrogels crosslinked through the different mechanisms. Data represents the mean ± SD. n = 3. Statistical analysis through two-way ANOVA and Tukey's HSD *post-hoc* test. * $p < 0.05$.

3.3. Swelling response

The swelling response of these hydrogels was examined to evaluate their suitability as scaffolds for wound healing applications.[46,52] By controlling the crosslinking density, swelling responses can be tuned and delivery kinetics of potentially encapsulated drugs can be controlled.[53,54] Softer hydrogels were able to swell to a greater extent than the stiffer hydrogels. Under basic conditions, the swelling response was significantly higher for all hydrogels compared to swelling under acidic conditions (Fig. 2). This swelling response plateaued at pH 9 for the mixed mode and all three dually crosslinked hydrogels, which were the stiffer gels (>15 kPa). Swelling was not statistically significant for the dually crosslinked hydrogels at pH 3 and at pH 5. One interesting finding was that at pH 7.4 and 9, the swelling response increased from the mixed mode gels to the ionic step growth gels and then decreased again. This may result from the Sr^{2+} interaction with the free carboxylic acid groups, mitigating the otherwise downward trend.

3.4. Degradation kinetics

Hydrogels should have degradation kinetics that are similar to the tissue regeneration rate in which they are implanted.[55,56] All of the hydrogels in this study were incubated in 0.1 mM NaOH to mimic accelerated degradation conditions (Fig. 3).

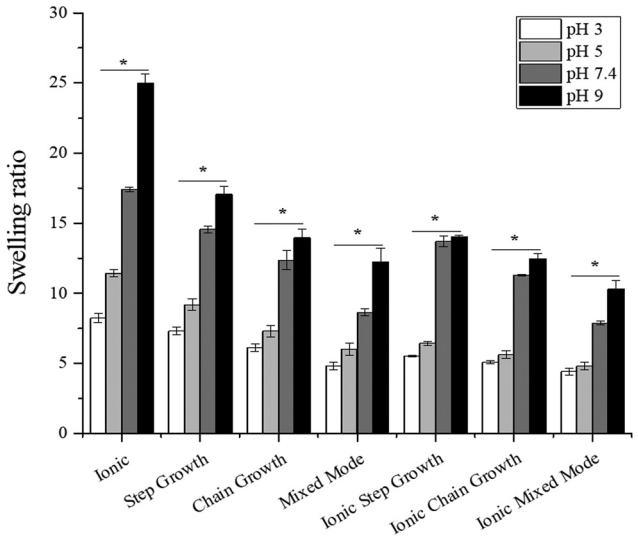

Fig. 2 Swelling response of the medium viscosity alginate hydrogels in a range of pH buffers. Hydrogels crosslinked through different mechanisms were swelled in pH 3, 5, 7.4, and 9 sodium acetate buffers. Data represents the mean ± SD. n = 3. Statistical analysis through two-way ANOVA and Tukey's HSD *post-hoc* test. * $p < 0.05$.

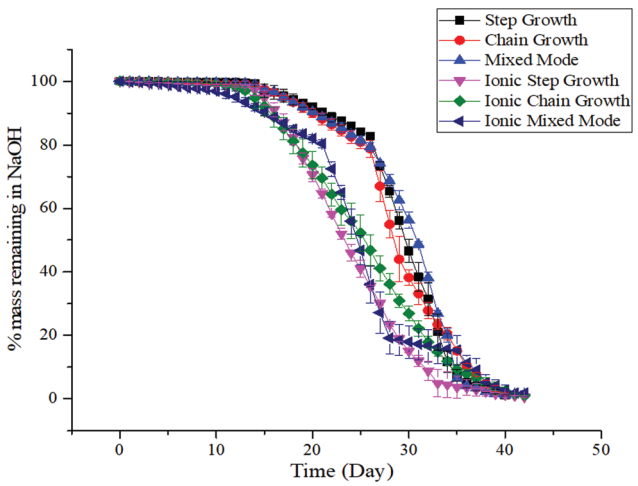

Fig. 3 Degradation response of medium viscosity alginate hydrogels under accelerated conditions. Alginate hydrogels were immersed in 0.1 mM NaOH to mimic accelerated degradation conditions. Data represents the mean ± SD. n = 3.

There were no statistical differences observed for the degradation kinetics of the covalently crosslinked hydrogels, with the three dually crosslinked hydrogels showing a relatively more stable response. The hydrogels degraded to 50% of their original mass over 31 ± 3 days for the covalently crosslinked hydrogels, while the half-life decreased to 25 ± 3 days for gels with additional ionic crosslinks.

3.5. Cytocompatibility of ALGMA hydrogels

One of the major prerequisites for any viable hydrogel used in biomedical applications is cytocompatibility.[18,57] Live/dead assays were conducted to evaluate the cytocompatibility of the different ALGMA hydrogels encapsulating NIH/3T3 fibroblasts. The encapsulated fibroblasts were imaged and compared after 48 hours of incubation, and the proliferation was normalized to the cells cultured on tissue culture plastic (Fig. 4). There was a steep increase in cell proliferation from step growth (27 ± 4%) to chain growth (51 ± 1%). Cell proliferation plateaued at ~60% for the dually crosslinked hydrogels, with values of 56 ± 2, 57 ± 1, and 62 ± 1% for the ionic step growth, ionic chain growth, and ionic mixed mode hydrogels, respectively. These results indicated that there may be a threshold hydrogel stiffness for the medium viscosity ALGMA hydrogels beyond which increased stiffness does not improve cell proliferation.

3.6. SHG microscopy

Encapsulated fibroblasts have been studied for their ability to synthesize collagen under diverse cell culture conditions.[58] SHG microscopy allows sensitive visualization of collagen secreted by these encapsulated cells as collagen is a non-centrosymmetric protein that is known to be SHG active. Collagen secretion levels were normalized to the background obtained by imaging non-cell laden hydrogel controls that had been incubated under identical conditions. Across the different hydrogel conditions there was an increase in collagen levels on day 7 compared to day 5 (Fig. 5). For all but one of the cell-hydrogel samples (ionic chain growth), the collagen levels on day 10 were significantly lower than the day 5 values. Collagen levels were positively correlated (R = 0.98) to the modulus of the hydrogel for all materials studied here (Fig. S2†). Ionic chain growth and ionic mixed mode hydrogels caused the fibroblasts to produce more collagen after 5 days of culture than the other hydrogels. There were significant differences observed for the increase in normalized collagen levels particularly for measurements taken on day 7 and day 10.

Collagen organization can influence cell morphology and proliferation.[59,60] It is also a biomarker for tumor progression.[61,62] In comparing the organization of the collagen secreted, and possibly rearranged by the fibroblasts,[62–65] there was an interesting trend in which softer gels resulted in more organized collagen, while stiffer gels resulted in less organized collagen (Fig. 6). Fig. 6A shows the orientation maps in which ROIs in which collagen was detected are represented with lines that depict the collagen orientation angle. These angles were color coded to better illustrate regions where collagen organization is similar. For the step growth gel, large regions of red and blue orientation angles can be seen. When the compressive modulus is increased to the mixed mode hydrogel, there do not appear to be clear regions of organization, suggesting that collagen organization is isotropic. To quantify collagen organization, the orientation angles in Fig. 6A were plotted as a histogram and fitted with a Gaussian. The full-width at half maximum (FWHM) was then plotted against the Young's modulus of the gels (Fig. 6B). Larger FWHMs signify disordered collagen while narrow dis-

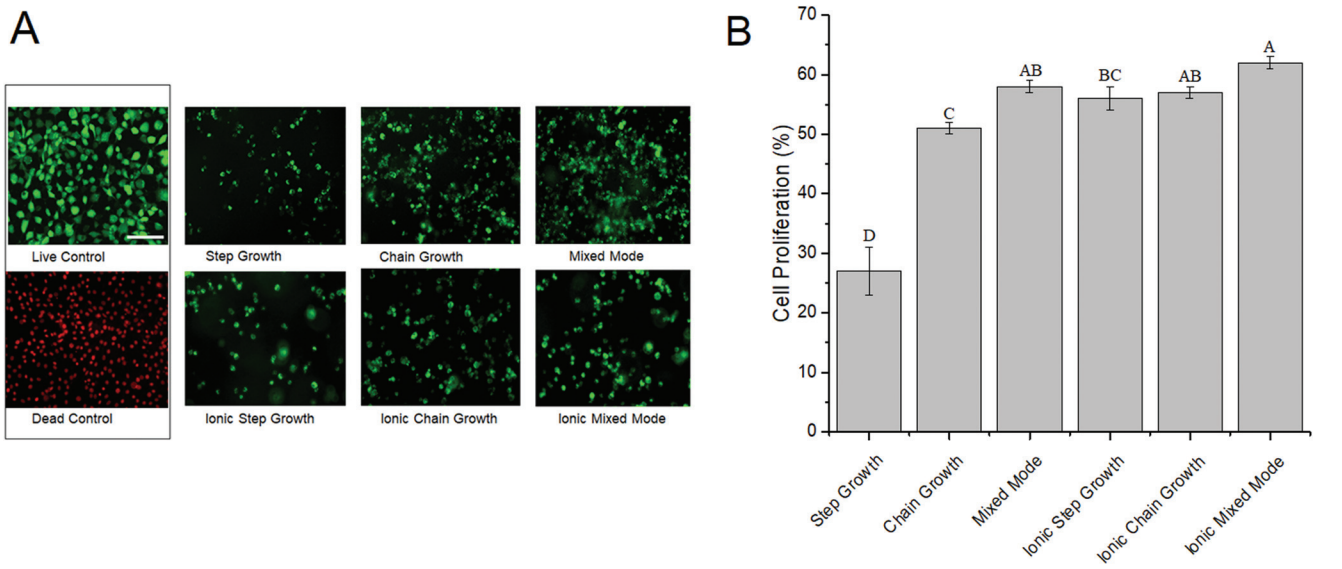

Fig. 4 Proliferation of NIH/3T3 cells encapsulated in medium viscosity alginate hydrogels. NIH/3T3 fibroblasts were mixed with ALGMA hydrogel solutions made from very low and medium viscosity alginic acid and crosslinked under different mechanisms. Cells cultured on tissue culture plastic served as controls. (A) Representative micrographs of live (green) and dead (red) cells cultured for 48 h. (B) Quantification of live and dead cells. Data represents the mean ± SD. $n = 6$. Statistical analysis through two-way ANOVA and Tukey's HSD *post-hoc* test. Bars with the same letter (A–G) are not statistically different ($p < 0.05$).

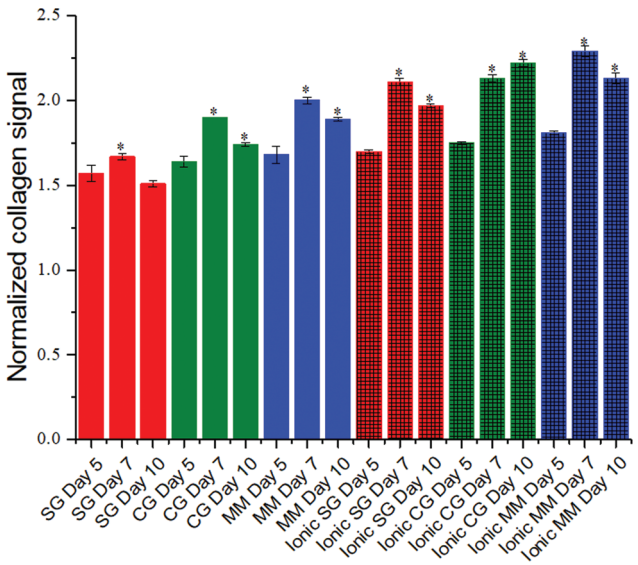

Fig. 5 Collagen secretion by NIH/3T3 cells encapsulated in medium viscosity alginate hydrogels was evaluated using SHG microscopy. Encapsulated NIH/3T3 fibroblasts were mixed with ALGMA and crosslinked. Collagen signal was normalized to the signal from the respective non-cell seeded hydrogel samples. Data represents the mean ± SD. $n = 3$. Statistical analysis was conducted for each hydrogel type through two-way ANOVA and Tukey's HSD *post-hoc* test. *$p < 0.05$ for samples compared to day 5 results. Red, green and blue colored bars represent the step growth, chain growth, and mixed mode crosslinking mechanisms. Dually crosslinked hydrogels are shown with additional crosshatch pattern on top of the original covalent crosslinking color.

tributions are more aligned and have smaller FWHMs. As seen in Fig. 6B, collagen organization decreases (FWHM increases) as the Young's modulus increases. This trend appears to reach a plateau or possibly decrease for ionic chain growth and ionic mixed mode gels, which have compressive moduli >20 kPa. The line in the figure is a guide for the eye. Mechanical properties have previously been shown to influence cell proliferation in which stiffer substrates corresponded to upregulation of protein secretion.[66] Conversely, previous studies have also shown that patterned protein presentation can be used to spatiotemporally tune stem cell differentiation, independent of the mechanics of the encapsulating hydrogel.[67] The empirical evidence presented on the influence of the hydrogel crosslinking method on collagen organization secreted by encapsulated fibroblasts demonstrates how materials can influence host responses to tissue engineered scaffolds.

4. Discussion

In this study, ALGMA hydrogels were synthesized through previously described protocols by reacting medium viscosity alginic acid precursor with methacrylic anhydride.[32] Key properties of these tunable hydrogels were analyzed including the compressive moduli, degradation kinetics, and swelling responses to different pH environments. The resulting empirical observations indicated that the medium viscosity ALGMA hydrogels are suitable for fabrication of cytocompatible scaffolds for studying collagen secretion and organizational changes by encapsulated fibroblasts.

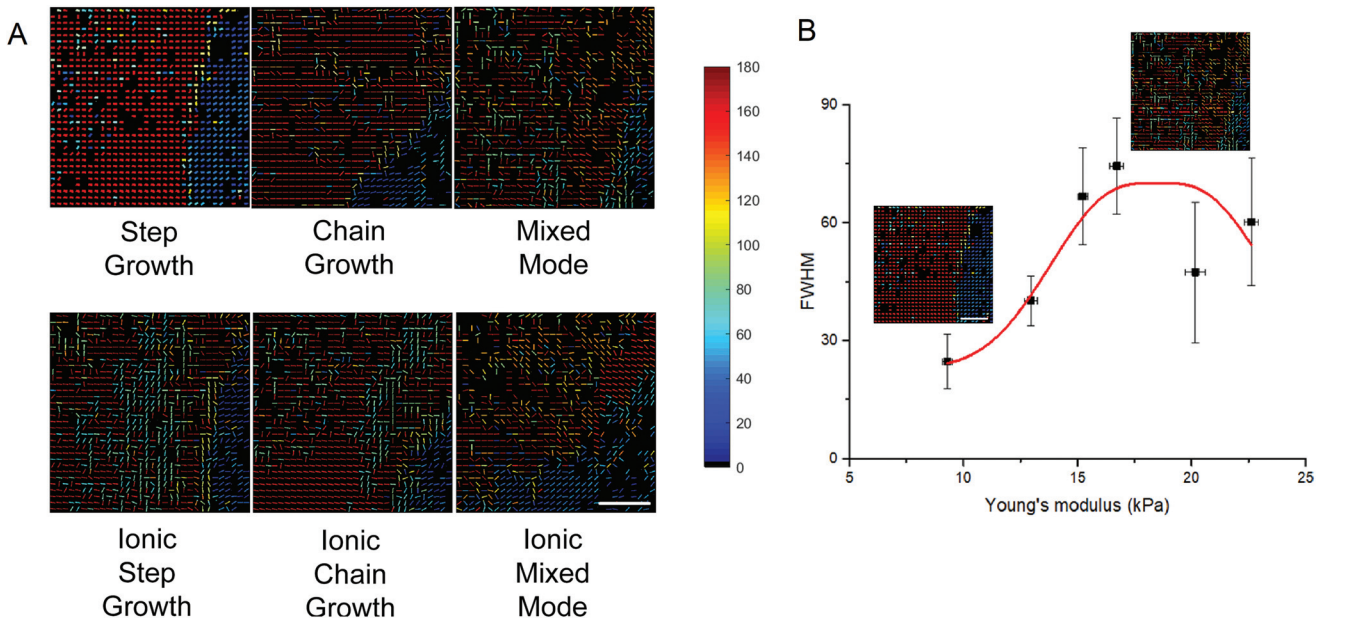

Fig. 6 Organization of collagen secreted by encapsulated fibroblasts in medium viscosity alginate hydrogels. Collagen secreted by NIH/3T3 fibroblasts encapsulated in the different alginate hydrogels were analyzed using SHG microscopy on day 10. (A) Maps of collagen organization in which the lines are placed on areas where collagen signal was detected, and the colors represent collagen organization angle. (B) Collagen organization mapped in terms of the FWHM against the Young's modulus of the alginate hydrogels. Data represents the mean ± SD. n = 3. The solid line is a guide for the eye indicating the trend for how collagen organization varies with changes in the modulus of crosslinked hydrogel. The legend to the organization of the collagen as seen in the heat-map is provided on the top right. The scale bar is 100 μm.

4.1. Methacrylated alginate hydrogels have tunable mechanical properties and are cytocompatible

Most cells are anchorage dependent and adhere to underlying substrates forming focal adhesions. This cell–substrate interaction senses substrate stiffness by the cell reaching out through the actin-myosin cytoskeleton and is critical to the subsequent expression of secreted proteins as well as differentiation to activated phenotypes.[8,50] Ionic, covalent, and a combination of the two (dual crosslinking) crosslinking mechanisms were employed to prepare medium viscosity ALGMA hydrogels with compressive moduli in the range of 8.3 ± 0.3 to 22.6 ± 0.3 kPa (Fig. 1). From these measurements, it is evident that there is a considerable influence from both the alginic acid precursor as well the crosslinking mechanism on the compressive moduli with our previously studied very low viscosity based ALGMA hydrogels restricted within a range of 0.5 ± 0.1 to 2.2 ± 0.1 kPa,[32] compared to the significantly stiffer ones synthesized here from medium viscosity precursors. The overall trend of the increase in compressive moduli conforms to the theory of rubber elasticity.[32,68] We are primarily concerned with how hydrogel properties can influence collagen organization. As such, this range of mechanical environments will allow us to disentangle trends between hydrogel stiffness and collagen alignment as this range of moduli traverses previously observed thresholds for fibroblasts to express actin stress fibers and differentiate to myofibroblasts.[69,70] Some studies have indicated the presence of an intermediate stage of proto-myofibroblasts that do not express α-smooth muscle actin, while still showing significantly higher overall actin expression.[71,72] Another study used chemically modified, soft alginate hydrogels with compressive moduli over the range of ~10 to 12 kPa, that showed low immune cell activation, and significantly reduced fibrotic response.[73]

Acute wound sites show rapid transition in pH from slightly acidic immediately after injury to basic conditions during granulation tissue formation, to more neutral levels upon reepithelialization.[74,75] Chronic wounds remain slightly alkali, which makes the wound site more susceptible to opportunistic pathogens.[75,76] Hence, an important aspect of designing biocompatible scaffolds from naturally derived, anionic polymers is utilizing their natural tendency to swell under basic pH conditions.[77,78] Responsive scaffolds that swell in alkaline pH can be used for delivering payloads of cytokines and chemokines that boost the natural wound healing process.[79,80] As the crosslinking density is inversely related to the swelling response,[68] it was expected that the softer purely ionically or covalently crosslinked hydrogels would swell more than the dually crosslinked gels. This trend held for previously studied very low viscosity ALGMA gels,[32] as well as the gels prepared here from medium viscosity alginic acid (Fig. 2). All the ALGMA hydrogels swelled the most at the pH 9 condition, which makes these viable materials for preparing scaffolds for chronic wound treatments. Further studies can be conducted to evaluate the kinetics of using such responsive hydrogels for drug delivery to chronic wounds, by studying the transport of clini-

cally relevant biomolecules from swollen hydrogels.[22] An environmentally responsive scaffold that can be tuned to deliver payloads of wound-healing relevant growth factors or patient-derived stromal cells could personalize wound care management with minimal adverse biological responses.[81,82]

The degradation of hydrogels results in decreased crosslink density over time.[83] Alginate hydrogels are very stable in PBS. Thus, to measure hydrolytic degradation, the ALGMA gels were incubated in a basic solution of 0.1 mM sodium hydroxide.[84,85] Covalently crosslinked ALGMA hydrogels derived from very low viscosity degraded to 50% of their original mass within 6 ± 1 days with dually crosslinking increasing the half-life to 13 ± 2 days.[32] The gels fabricated here were almost 5 times as stable, with half-lives of 31 ± 3 days (Fig. 3). However, dually crosslinking the medium viscosity gels did not increase the half-life (25 ± 3 days). Ideally, degradation kinetics of the scaffold should match tissue regeneration rates. Potential inflammatory or fibrotic responses can result if these rates are not equivalent.[86] The particular combination of ionic and covalent crosslinking on catechol-modified alginate hydrogels has been demonstrated as a viable mechanism for preparation of mechanically congruent, viable and cytocompatible scaffolds.[87] In this study, it was observed that the dually crosslinked hydrogels can be synthesized with tunable structural integrity that can remain intact for longer incubation and potentially prevent implant rejection scenarios.

Scaffolds must be cytocompatible.[88] NIH/3T3 cells showed no cell death when encapsulated in the different crosslinked ALGMA hydrogels (Fig. 4). Additionally, the encapsulated cells had cell proliferation above 50% compared to the controls of tissue culture plastic (TCP), with the exception of step-growth gels. When looking at the compressive moduli and cell proliferation, it appears that there was a threshold compressive modulus beyond which the cell proliferation showed few significant changes with increased crosslinking density. 3D encapsulation of cells allows for relatively better approximations of the natural *in vivo* conditions, as compared to surface seeding studies.[18] Comparing the cell morphology in the live/dead assay, there were no differences for the different hydrogel environments which agrees with Huebsch *et al.*[66] In an effort to decouple the mechanical effects of 3D modified alginate matrices from the available calcium ions on the morphology of human mesenchymal stem cells (hMSCs, which are similar in many ways to fibroblasts), the cells were encapsulated in alginate hydrogels of varying Young's modulus and fixed concentration of the RGD motif that was used to increase cell adhesion. There were no significant changes in morphology observed when cultured for 2 h, 24 h and even one week under encapsulated conditions. Such studies indicate the complexity in using nanoporous cell encapsulation hydrogels such as alginate for studying the changes in cell morphological responses. The plateaued trend of the cell proliferation to the dually crosslinked hydrogels introduces the possibility that once the ALGMA hydrogels are uniformly crosslinked above 20 kPa, it be possible to disentangle the effect of gelation mechanism and the rigidity to determine which factor holds greater significance on cellular responses.[89,90]

4.2. Alginate compressive modulus influences collagen organization

Fibroblasts have mechanical memory regarding the stiffness of the substrates they are cultured on, particularly with respect to how they differentiate to myofibroblasts which has been positively correlated to over-secretion of collagen I.[49,58,91] The viscoelastic nature of natural tissues has been replicated to a limited extent in alginate hydrogels for better understanding of cell interaction that can inform design of effective implants.[92–94] Qualitative as well as quantitative analysis of the secreted collagen using SHG microscopy has allowed for an informed rational design of biocompatible materials.[95,96] Here, we see a significant increase of the collagen levels on day 7 for all hydrogel conditions compared to day 5 (Fig. 5). This was expected as protein deposition typically increases with culture time. The overall timeline can vary based on several factors such as size, shape and topography of the environment.[97] The positive correlation of the collagen levels to the modulus of the underlying substrate conformed to previous studies in which stiffer substrates cause stromal cells to secrete more ECM proteins particularly around day 7 to day 10.[57,98] The decrease in collagen levels beyond day 7 may result from an increase in MMP-13 (collagenase).[98] These results could also indicate an upregulation in overall cell activity which may be a precursor for fibroblast-to-myofibroblast differentiation, particularly in the stiffer microenvironments.[99] Similarly, Huebsch *et al.* found that stiffer alginate hydrogels encapsulating hMSCs instigated osteogenic differentiation, with a biphasic influence of the modulus on ECM secretion.[66] Beyond just the quantification of the collagen levels, it is of great importance to understand the influence of collagen organization.[59] There is a dearth of studies conducted on the tunability of local collagen organization using sensitive visualization techniques.

The organization of collagen in the ECM influences the remodeling of wounds,[100] as well as acceptance of implants.[95] Aligned collagen is found in specific natural environments such as mammalian tendons as well as cornea.[101,102] Stochastic collagen is present in natural dermis.[103] Keeping collagen alignment in mind, we can determine how materials properties will change cellular responses and this understanding can improve scaffold design for tissue repair in different organs.[22] Collagen angles were measured using SHG and were plotted using a heat map to better visualize regions of organization. Softer step growth gels (~10 kPa) can be seen as having a lower FWHM, which indicates that the hydrogel resulted in more aligned collagen. This can be visualized in the heat map in which there are large regions of collagen having the same orientation angle. The FWHM of collagen decreases with increasing compressive modulus, which means the collagen is more isotropic. The heat map shows that there is a large variation in collagen angles for the ionic step growth condition (~15 kPa) (Fig. 6A). This suggests that not only mechanical

stiffness of the underlying substrate influences collagen response, necessitating further research on disentangling the influence of crosslinking mechanisms on cell interactions. As this study is limited to collagen based analysis, future studies on the expression of FAK and MAPK expression along with quantified immunocytochemical staining of cells cultured in or on such scaffolds could further elucidate the mechanism that is causing collagen organization.[104–106] This study provides further development of SHG microscopy as a platform for visualizing the influence of materials properties in tunable hydrogels on how cells sense their local microenvironment.

5. Conclusions

We successfully fabricated methacrylated alginate hydrogels from medium viscosity alginic acid through ionic, covalent, and a combination of ionic and covalent crosslinking mechanisms. These mechanisms yielded a range of hydrogels that were stiffer, pH responsive, as well as significantly more robust under accelerated degradation conditions of incubation compared to hydrogels fabricated from very low viscosity alginate. NIH/3T3 fibroblasts encapsulated in these hydrogels showed no cell death and a preferred threshold stiffness above which cell proliferation was >60% compared to TCP controls. Collagen secretion in response to the encapsulation conditions was positively correlated with the modulus for all environments. Collagen was more isotropic for the mixed mode and ionic step growth conditions, whereas the softer gels resulted in more anisotropic organization. The detailed characterization of the influence of crosslinking mechanisms for these responsive ALGMA hydrogels indicates the need for including it as an important factor for the fabrication of tissue engineering scaffolds.

Conflicts of interest

There are no conflicts to declare.

Acknowledgements

This work was supported by the Roy J. Carver Charitable Trust Grant No. 13-4265.

References

1 D. E. Discher, P. A. Janmey and Y. Wang, Tissue Cells Feel and Respond to the Stiffness of Their Substrate, *Science*, 2005, **310**, 1139–1143.
2 C. M. Nelson and M. J. Bissell, Of Extracellular Matrix, Scaffolds, and Signaling: Tissue Architecture Regulates Development, Homeostasis, and Cancer, *Annu. Rev. Cell Dev. Biol.*, 2006, **22**, 287–309.
3 M. W. Tibbitt and K. S. Anseth, Hydrogels as extracellular matrix mimics for 3D cell culture, *Biotechnol. Bioeng.*, 2009, **103**, 655–663.
4 F. Rosso, A. Giordano, M. Barbarisi and A. Barbarisi, From Cell-ECM Interactions to Tissue Engineering, *J. Cell. Physiol.*, 2004, **199**, 174–180.
5 J. M. Aamodt and D. W. Grainger, Extracellular matrix-based biomaterial scaffolds and the host response, *Biomaterials*, 2016, **86**, 68–82.
6 A. Jikko, S. E. Harris, D. Chen, D. L. Mendrick and C. H. Damsky, Collagen Integrin Receptors Regulate Early Osteoblast Differentiation Induced by BMP-2, *J. Bone Miner. Res.*, 1999, **14**, 1075–1083.
7 M. V. Plikus, *et al.*, Regeneration of fat cells from myofibroblasts during wound healing, *Science*, 2017, **8792**, 1–12.
8 T. Yeung, *et al.*, Effects of substrate stiffness on cell morphology, cytoskeletal structure, and adhesion, *Cell Motil. Cytoskeleton*, 2005, **60**, 24–34.
9 D. E. Discher, *et al.*, Matrix Mechanosensing: From Scaling Concepts in 'Omics Data to Mechanisms in the Nucleus, Regeneration, and Cancer, *Annu. Rev. Biophys.*, 2017, **46**, 295–315.
10 K. Burridge and C. Guilluy, Focal adhesions, stress fibers and mechanical tension, *Exp. Cell Res.*, 2016, **343**, 14–20.
11 P. F. Lee, Y. Bai, R. L. Smith, K. J. Bayless and a. T. Yeh, Angiogenic responses are enhanced in mechanically and microscopically characterized, microbial transglutaminase crosslinked collagen matrices with increased stiffness, *Acta Biomater.*, 2013, **9**, 7178–7190.
12 I. Stamenkovic, Extracellular matrix remodelling: the role of matrix metalloproteinases, *J. Pathol.*, 2003, **200**, 448–464.
13 G. C. Gurtner, S. Werner, Y. Barrandon and M. T. Longaker, Wound repair and regeneration, *Nature*, 2008, **453**, 314–321.
14 P. Bao, *et al.*, The Role of Vascular Endothelial Growth Factor in Wound Healing, *J. Surg. Res.*, 2009, **153**, 347–358.
15 M. Loeffler, J. A. Krüger, A. G. Niethammer and R. A. Reisfeld, Targeting tumor-associated fibroblasts improves cancer chemotherapy by increasing intratumoral drug uptake, *J. Clin. Invest.*, 2006, **116**, 1955–1962.
16 J. D. Bryers, C. M. Giachelli and B. D. Ratner, Engineering biomaterials to integrate and heal: The biocompatibility paradigm shifts, *Biotechnol. Bioeng.*, 2012, **109**, 1898–1911.
17 R. H. Harrison, J.-P. St-Pierre and M. M. Stevens, Tissue Engineering and Regenerative Medicine: A Year in Review, *Tissue Eng., Part B*, 2014, **20**, 1–16.
18 P. M. Kharkar, K. L. Kiick and A. M. Kloxin, Designing degradable hydrogels for orthogonal control of cell microenvironments, *Chem. Soc. Rev.*, 2013, **42**, 7335–7372.
19 S. R. Peyton, C. B. Raub, V. P. Keschrumrus and A. J. Putnam, The use of poly (ethylene glycol) hydrogels to investigate the impact of ECM chemistry and mech-

anics on smooth muscle cells, *Biomaterials*, 2006, **27**, 4881–4893.
20 O. Jeon, C. Powell, S. M. Ahmed and E. Alsberg, Biodegradable, photocrosslinked alginate hydrogels with independently tailorable physical properties and cell adhesivity, *Tissue Eng., Part A*, 2010, **16**, 2915–2925.
21 K. Y. Lee and D. J. Mooney, Alginate: Properties and biomedical applications, *Prog. Polym. Sci.*, 2012, **37**, 106–126.
22 O. Jeon, C. Powell, L. D. Solorio, M. D. Krebs and E. Alsberg, Affinity-based growth factor delivery using biodegradable, photocrosslinked heparin-alginate hydrogels, *J. Controlled Release*, 2011, **154**, 258–266.
23 J. A. Rowley, G. Madlambayan and D. J. Mooney, Alginate hydrogels as synthetic extracellular matrix materials, *Biomaterials*, 1999, **20**, 45–53.
24 A. E. Baer, J. Y. Wang, V. B. Kraus and L. A. Setton, Collagen gene expression and mechanical properties of intervertebral disc cell-alginate cultures, *J. Orthop. Res.*, 2001, **19**, 2–10.
25 W. L. Chen, *et al.*, Second harmonic generation ?? tensor microscopy for tissue imaging, *Appl. Phys. Lett.*, 2009, **94**, 2007–2010.
26 A. I. Chou, S. O. Akintoye and S. B. Nicoll, Photo-cross-linked alginate hydrogels support enhanced matrix accumulation by nucleus pulposus cells in vivo, *Osteoarthr. Cartil.*, 2009, **17**, 1377–1384.
27 M. Kastellorizios, N. Tipnis and D. J. Burgess, Foreign body reaction to subcutaneous implants, *Adv. Exp. Med. Biol.*, 2015, **865**, 93–108.
28 S. Gay, J. Vijanto, J. Raekallio and R. Penttinen, Collagen types in early phases of wound healing in children, *Acta Chir. Scand.*, 1978, **144**, 205–211.
29 G. Gabbiani, The myofibroblast in wound healing and fibrocontractive diseases, *J. Pathol.*, 2003, **200**, 500–503.
30 H. P. Ehrlich, *et al.*, Morphological and immunochemical differences between keloid and hypertrophic scar, *Am. J. Pathol.*, 1994, **145**, 105–113.
31 R. Cicchi, *et al.*, Scoring of collagen organization in healthy and diseased human dermis by multiphoton microscopy, *J. Biophotonics*, 2010, **3**, 34–43.
32 A. Boddupalli and K. M. Bratlie, Collagen organization deposited by fibroblasts encapsulated in pH responsive methacrylated alginate hydrogels, *J. Biomed. Mater. Res., Part A*, 2018, **106**, 2934–2943.
33 H. Shih and C.-C. Lin, Cross-Linking and Degradation of Step-Growth Hydrogels Formed by Thiol-Ene Photoclick Chemistry, *Biomacromolecules*, 2012, **13**, 2003–2012.
34 I. Mironi-harpaz, D. Yingquan, S. Venkatraman and D. Seliktar, Photopolymerization of cell-encapsulating hydrogels: Crosslinking efficiency versus cytotoxicity, *Acta Biomater.*, 2012, **8**, 1838–1848.
35 S. K. Reddy, K. S. Anseth and C. N. Bowman, Modeling of network degradation in mixed step-chain growth polymerizations, *Polymer*, 2005, **46**, 4212–4222.
36 C. N. Salinas and K. S. Anseth, Mixed Mode Thiol - Acrylate Photopolymerizations for the Synthesis of PEG - Peptide Hydrogels, *Macromolecules*, 2008, **41**, 6019–6026.
37 L. Zhu and K. M. Bratlie, pH sensitive methacrylated chitosan hydrogels with tunable physical and chemical properties, *Biochem. Eng. J.*, 2018, **132**, 38–46.
38 J. E. Samorezov, C. M. Morlock and E. Alsberg, Dual Ionic and Photo-Crosslinked Alginate Hydrogels for Micropatterned Spatial Control of Material Properties and Cell Behavior, *Bioconjugate Chem.*, 2015, **26**, 1339–1347.
39 P. Marques, M. E. Gomes, A. Khademhosseini and C. Link, Photocrosslinkable Kappa-Carrageenan Hydrogels for Tissue Engineering Applications Accessed, *Adv. Healthcare Mater.*, 2018, **2**, 895–907.
40 H. Tan, H. Li, P. J. Rubin and K. G. Marra, Controlled Gelation and Degradation Rates of Injectable Hyaluronic Acid-based Hydrogels through a Double Crosslinking Strategy, *J. Tissue Eng. Regener. Med.*, 2011, **5**, 790–797.
41 K. Stuart and A. Panitch, Characterization of gels composed of blends of collagen l, collagen III, and chondroitin sulfate, *Biomacromolecules*, 2009, **10**, 25–31.
42 X. G. Chen, Z. Wang, W. S. Liu and H. J. Park, The effect of carboxymethyl-chitosan on proliferation and collagen secretion of normal and keloid skin fibroblasts, *Biomaterials*, 2002, **23**, 4609–4614.
43 A. Boddupalli and K. M. Bratlie, Multimodal imaging of harmonophores and application of high content imaging for early cancer detection, *Mater. Discovery*, 2016, **1**, 10–20.
44 P. J. Campagnola and L. M. Loew, Second-harmonic imaging microscopy for visualizing biomolecular arrays in cells, tissues and organisms, *Nat. Biotechnol.*, 2003, **21**, 1356–1360.
45 M. Olderøy, *et al.*, Biochemical and structural characterization of neocartilage formed by mesenchymal stem cells in alginate hydrogels, *PLoS One*, 2014, **9**, e101096.
46 A. I. Chou and S. B. Nicoll, Characterization of photocrosslinked alginate hydrogels for nucleus pulposus cell encapsulation, *J. Biomed. Mater. Res., Part A*, 2009, **91**, 187–194.
47 H. C. Bygd and K. M. Bratlie, The effect of chemically modified alginates on macrophage phenotype and biomolecule transport, *J. Biomed. Mater. Res., Part A*, 2016, **104**, 1707–1719.
48 D. W. Hutmacher, Scaffolds in tissue engineering bone and cartilage, *Biomaterials*, 2000, **21**, 2529–2543.
49 J. L. Balestrini, S. Chaudhry, V. Sarrazy, A. Koehler and B. Hinz, The mechanical memory of lung myofibroblasts, *Integr. Biol.*, 2012, **4**, 410.
50 R. G. Wells, The role of matrix stiffness in regulating cell behavior, *Hepatology*, 2008, **47**, 1394–1400.
51 F. Liu, *et al.*, Feedback amplification of fibrosis through matrix stiffening and COX-2 suppression, *J. Cell Biol.*, 2010, **190**, 693–706.
52 B. V. Slaughter, S. S. Khurshid, O. Z. Fisher, A. Khademhosseini and N. A. Peppas, Hydrogels in Regenerative Medicine, *Adv. Mater.*, 2009, **21**, 3307–3329.

53 K. S. Anseth, C. N. Bowman and L. Brannon-Peppas, Mechanical properties of hydrogels and their experimental determination, *Biomaterials*, 1996, **17**, 1647–1657.
54 K. Podual, F. J. Doyle and N. A. Peppas, Preparation and dynamic response of cationic copolymer hydrogels containing glucose oxidase, *Polymer*, 2000, **41**, 3975–3983.
55 C. R. Almeida, *et al.*, Impact of 3-D printed PLA- and chitosan-based scaffolds on human monocyte/macrophage responses: Unraveling the effect of 3-D structures on inflammation, *Acta Biomater.*, 2014, **10**, 613–622.
56 A. E. Rydholm, C. N. Bowman and K. S. Anseth, Degradable thiol-acrylate photopolymers: Polymerization and degradation behavior of an in situ forming biomaterial, *Biomaterials*, 2005, **26**, 4495–4506.
57 A. M. Kloxin, A. M. Kasko, C. N. Salinas and K. S. Anseth, Photodegradable hydrogels for dynamic tuning of physical and chemical properties, *Science*, 2009, **324**, 59–63.
58 D. J. Holt, L. M. Chamberlain and D. W. Grainger, Cell-cell signaling in co-cultures of macrophages and fibroblasts, *Biomaterials*, 2010, **31**, 9382–9394.
59 T. Yasui, Y. Tohno and T. Araki, Characterization of collagen orientation in human dermis by two-dimensional second-harmonic-generation polarimetry, *J. Biomed. Opt.*, 2004, **9**, 259.
60 D. P. Berry, K. G. Harding, M. R. Stanton, B. Jasani and H. P. Ehrlich, Human wound contraction: collagen organization, fibroblasts, and myofibroblasts, *Plast. Reconstr. Surg.*, 1998, **102**, 124–131; discussion 132–134.
61 M. W. Conklin, *et al.*, Aligned collagen is a prognostic signature for survival in human breast carcinoma, *Am. J. Pathol.*, 2011, **178**, 1221–1232.
62 P. P. Provenzano, *et al.*, Collagen reorganization at the tumor-stromal interface facilitates local invasion, *BMC Med.*, 2006, **4**, 38.
63 P. P. M. Van Zuijlen, *et al.*, Collagen morphology in human skin and scar tissue: No adaptations in response to mechanical loading at joints, *Burns*, 2003, **29**, 423–431.
64 H. Cook, P. Stephens, K. J. Davies, K. G. Harding and D. W. Thomas, Defective extracellular matrix reorganization by chronic wound fibroblasts is associated with alterations in TIMP-1, TIMP-2, and MMP-2 activity, *J. Invest. Dermatol.*, 2000, **115**, 225–233.
65 F. Grinnell, Fibroblast-collagen-matrix contraction: growth-factor signalling and mechanical loading, *Trends Cell Biol.*, 2000, **10**, 362–365.
66 N. Huebsch, *et al.*, Harnessing traction-mediated manipulation of the cell/matrix interface to control stem-cell fate, *Nat. Mater.*, 2010, **9**, 518–526.
67 C. A. DeForest and D. A. Tirrell, A photoreversible protein-patterning approach for guiding stem cell fate in three-dimensional gels, *Nat. Mater.*, 2015, **14**, 523–531.
68 P. J. Flory and J. Rehner, Statistical mechanics of cross-linked polymer networks II. Swelling, *J. Chem. Phys.*, 1943, **11**, 521–526.
69 J. J. Tomasek, G. Gabbiani, B. Hinz, C. Chaponnier and R. a. Brown, Myofibroblasts and mechano-regulation of connective tissue remodelling, *Nat. Rev. Mol. Cell Biol.*, 2002, **3**, 349–363.
70 B. Hinz, The myofibroblast: Paradigm for a mechanically active cell, *J. Biomech.*, 2010, **43**, 146–155.
71 R. J. McAnulty, Fibroblasts and myofibroblasts: Their source, function and role in disease, *Int. J. Biochem. Cell Biol.*, 2007, **39**, 666–671.
72 C. Chaponnier and G. Gabbiani, Tissue repair, contraction, and the myofibroblast factors involved in myofibroblastic, *Wound Repair Regen.*, 2005, **13**, 7–12.
73 A. J. Vegas, *et al.*, Combinatorial hydrogel library enables identification of materials that mitigate the foreign body response in primates, *Nat. Biotechnol.*, 2016, **34**, 345–352.
74 L. A. Schneider, A. Korber, S. Grabbe and J. Dissemond, Influence of pH on wound-healing: A new perspective for wound-therapy?, *Arch. Dermatol. Res.*, 2007, **298**, 413–420.
75 G. Gethin, The significance of surface pH in chronic wounds, *Wounds*, 2007, **3**, 52–56.
76 S. Schreml, *et al.*, The impact of the pH value on skin integrity and cutaneous wound healing, *J. Eur. Acad. Dermatol. Venereol.*, 2010, **24**, 373–378.
77 K. Y. Lee, *et al.*, Controlling mechanical and swelling properties of alginate hydrogels independently by cross-linker type and cross-linking density, *Macromolecules*, 2000, **33**, 4291–4294.
78 A. R. Khare and N. A. Peppas, Swelling/deswelling of anionic copolymer gels, *Biomaterials*, 1995, **16**, 559–567.
79 S. I. Jeong, O. Jeon, M. D. Krebs, M. C. Hill and E. Alsberg, Biodegradable photo-crosslinked alginate nanofibre scaffolds with tuneable physical properties, cell adhesivity and growth factor release, *Eur. Cells Mater.*, 2012, **24**, 331–343.
80 G. Lokhande, *et al.*, Nanoengineered injectable hydrogels for wound healing application, *Acta Biomater.*, 2018, **70**, 35–47.
81 P. Eiselt, J. Yeh, R. K. Latvala, L. D. Shea and D. J. Mooney, Porous carriers for biomedical applications based on alginate hydrogels, *Biomaterials*, 2000, **21**, 1921–1927.
82 A. W. Chan, R. A. Whitney and R. J. Neufeld, Semisynthesis of a controlled stimuli-responsive alginate hydrogel, *Biomacromolecules*, 2009, **10**, 609–616.
83 C. Cha, R. E. Kohman and H. Kong, Biodegradable polymer crosslinker: independent control of stiffness, toughness, and hydrogel degradation rate, *Adv. Funct. Mater.*, 2009, **19**, 3056–3062.
84 M. B. Browning, S. N. Cereceres, P. T. Luong and E. M. Cosgriff-Hernandez, Determination of the in vivo degradation mechanism of PEGDA hydrogels, *J. Biomed. Mater. Res., Part A*, 2014, **102**, 4244–4251.
85 D. F. Coutinho, *et al.*, Modified Gellan Gum hydrogels with tunable physical and mechanical properties, *Biomaterials*, 2010, **31**, 7494–7502.
86 D. L. M. Dinnes, J. P. Santerre and R. S. Labow, Influence of biodegradable and non-biodegradable material surfaces on the differentiation of human mono-

cyte-derived macrophages, *Differentiation*, 2008, **76**, 232–244.
87 S. H. Hong, *et al.*, STAPLE: Stable Alginate Gel Prepared by Linkage Exchange from Ionic to Covalent Bonds, *Adv. Healthcare Mater.*, 2016, **5**, 75–79.
88 O. Jeon, K. H. Bouhadir, J. M. Mansour and E. Alsberg, Photocrosslinked alginate hydrogels with tunable biodegradation rates and mechanical properties, *Biomaterials*, 2009, **30**, 2724–2734.
89 E. R. Ruskowitz and C. A. Deforest, Photoresponsive biomaterials for targeted drug delivery and 4D cell culture, *Nat. Rev. Mater.*, 2018, **3**, 17087.
90 S. Nemir, H. N. Hayenga and J. L. West, PEGDA Hydrogels With Patterned Elasticity: Novel Tools for the Study of Cell Response to Substrate Rigidity, *Biotechnol. Bioeng.*, 2010, **105**, 636–644.
91 G. S. A. Boersema, N. Grotenhuis, Y. Bayon, J. F. Lange and Y. M. Bastiaansen-Jenniskens, The Effect of Biomaterials Used for Tissue Regeneration Purposes on Polarization of Macrophages, *BioRes. Open Access*, 2016, **5**, 6–14.
92 O. Chaudhuri, *et al.*, Substrate stress relaxation regulates cell spreading, *Nat. Commun.*, 2015, **6**, 6365.
93 O. Chaudhuri, *et al.*, Hydrogels with tunable stress relaxation regulate stem cell fate and activity, *Nat. Mater.*, 2015, **15**, 326–334.
94 C. Lee, *et al.*, Bioinspired, calcium-free alginate hydrogels with tunable physical and mechanical properties and improved biocompatibility, *Biomacromolecules*, 2013, **14**, 2004–2013.
95 D. Akilbekova and K. M. Bratlie, Quantitative characterization of collagen in the fibrotic capsule surrounding implanted polymeric microparticles through second harmonic generation imaging, *PLoS One*, 2015, **10**, 1–17.
96 H. C. Bygd, D. Akilbekova, A. Muñoz, K. D. Forsmark and K. M. Bratlie, Poly-l-arginine based materials as instructive substrates for fibroblast synthesis of collagen, *Biomaterials*, 2015, **63**, 47–57.
97 J. M. Anderson, Biological Responses to Materials, *Annu. Rev. Mater. Res.*, 2001, **31**, 81–110.
98 C. N. Salinas and K. S. Anseth, The enhancement of chondrogenic differentiation of human mesenchymal stem cells by enzymatically regulated RGD functionalities, *Biomaterials*, 2008, **29**, 2370–2377.
99 F. Klingberg, B. Hinz and E. S. White, The myofibroblast matrix: Implications for tissue repair andfibrosis, *J. Pathol.*, 2013, **229**, 298–309.
100 R. S. English and P. D. Shenefelt, Keloids and hypertrophic scars, *Dermatol. Surg.*, 1999, **25**, 631–638.
101 P. J. Su, *et al.*, The discrimination of type I and type II collagen and the label-free imaging of engineered cartilage tissue, *Biomaterials*, 2010, **31**, 9415–9421.
102 K. M. Meek and C. Boote, The organization of collagen in the corneal stroma, *Exp. Eye Res.*, 2004, **78**, 503–512.
103 H. A. Linares, C. W. Kischer, M. Dobrkovsky and D. L. Larson, The histiotypic organization of collagen of the hypertrophic scar in humans, *J. Invest. Dermatol.*, 1972, **59**, 323–332.
104 J. M. Goffin, *et al.*, Focal adhesion size controls tension-dependent recruitment of ??-smooth muscle actin to stress fibers, *J. Cell Biol.*, 2006, **172**, 259–268.
105 B. Trappmann, *et al.*, Extracellular-matrix tethering regulates stem-cell fate, *Nat. Mater.*, 2012, **11**, 742–742.
106 D. H. Kim, *et al.*, Mechanosensitivity of fibroblast cell shape and movement to anisotropic substratum topography gradients, *Biomaterials*, 2009, **30**, 5433–5444.